INSTITUTE OF PHYSICS PUBLISHING NONLINEARITY

Nonlinearity **16** (2003) 1875–1898 PII: S0951-7715(03)59211-8

Formation of discontinuities in flux-saturated degenerate parabolic equations

Alina Chertock[1], **Alexander Kurganov**[2] **and Philip Rosenau**[3]

[1] Department of Mathematics, North Carolina State University, Raleigh, NC 27695, USA
[2] Department of Mathematics, Tulane University, New Orleans, LA 70118, USA
[3] School of Mathematical Sciences, Tel Aviv University, Tel Aviv 69978, Israel

E-mail: chertock@math.ncsu.edu, kurganov@math.tulane.edu and rosenau@post.tau.ac.il

Received 5 February 2003, in final form 20 May 2003
Published 19 August 2003
Online at stacks.iop.org/Non/16/1875

Recommended by R Krasny

Abstract

We endow the nonlinear degenerate parabolic equation used to describe propagation of thermal waves in plasma or in a porous medium, with a mechanism for flux saturation intended to correct the nonphysical gradient-flux relations at high gradients. We study both analytically and numerically the resulting equation: $u_t = [u^n Q(g(u)_x)]_x, n > 0$, where Q is a bounded increasing function. This model reveals that for $n > 1$ the motion of the front is controlled by the saturation mechanism and instead of the typical infinite gradients resulting from the linear flux-gradients relations, $Q \sim u_x$, we obtain a sharp, shock-like front, typically associated with nonlinear hyperbolic phenomena. We prove that if the initial support is compact, independently of the smoothness of the initial datum inside the support, a sharp front discontinuity forms in a finite time, and until then the front does not expand.

Mathematics Subject Classification: 35K65, 35B65, 35B40

1. Introduction

This paper is devoted to the study of a model equation obtained when the nonlinear degenerate parabolic equation used to describe propagation of thermal waves in plasma or flow in porous medium (the so-called 'porous medium equation'), is endowed with a saturation mechanism intended to correct the nonphysical gradient-flux relations at high gradients. It is an extension of our previous studies of saturation mechanism being imposed on linear diffusion [26, 25]. The considered model equation is

$$u_t = [u^n Q(g(u)_x)]_x, \qquad n > 0, \tag{1.1}$$

0951-7715/03/061875+24$30.00

where $g(u)$ is a smooth function, and $Q(s)$ is a bounded increasing function satisfying $Q(0) = 0$ and $Q'(s) > 0\ \forall s$.

A typical example of Q is

$$Q(s) = \frac{s}{\sqrt{1+s^2}}, \tag{1.2}$$

which, if $s = u_x$, also corresponds to a mean-curvature-type diffusion flux. Of course, for the linear flux case, wherein $Q \sim u_x$, the problem reduces to the well-known case often referred to as the porous medium equation. The model equation studied in this paper was introduced some time ago by one of us [23, 24].

We mention a similar equation,

$$u_t = [\varphi(u)Q(u_x)]_x, \tag{1.3}$$

subject to a monotone increasing initial datum which was studied in [12]. In that work the notion of a weak solution of (1.3) was defined and the existence of a (possibly discontinuous) weak solution was proved which, in general, is not unique. In [12, 15] it was also shown that there exists a unique weak solution, which satisfies Oleinik's entropy condition, and that this solution can be obtained via a vanishing viscosity approximation.

Though the boundedness of the flux function Q is a fundamental property of real physical systems, this feature is almost always lost in the weakly nonlinear, small gradients expansions, underlying the derivation of most, if not all, continuum models. The rationale behind the particular form of the saturated diffusion used in this work is discussed in appendix A. The synthesized form of the saturation flux is in a sense a Padé approximant which connects universal features present at both very small and very large fluxes. Consequently, there is a certain arbitrariness in the choice of the saturating flux function Q. It is thus meaningful that as a byproduct of our studies, we obtain that insofar as Q is monotone in gradients and saturates at a proper rate, the particulars of the flux function are to large extent of secondary importance. However, as in the standard porous medium equation (the linear flux case),

$$u_t = [u^n u_x]_x, \tag{1.4}$$

the choice on n in (1.1) is important.

As mentioned above, our previous studies were confined to the case of $g(u) = u$, $n = 0$:

$$u_t = [Q(u_x)]_x. \tag{1.5}$$

Equation (1.5) has the remarkable property of delaying the resolution of discontinuities shown in [26, 12]. Namely, if the initial datum, $u_0(x) := u(x, 0)$, is discontinuous at some point x_0, and if the integral $\int_0^\infty s\,Q'(s)\,\mathrm{d}s$ is finite, then there exists a finite time $T > 0$ such that the solution $u(x, t)$ becomes continuous at (x_0, t) only after $t \geqslant T$. In any case, all initial discontinuities will be smoothed out after a certain time.

If a nonlinear convection is added to (1.5),

$$u_t + f(u)_x = [Q(u_x)]_x, \tag{1.6}$$

the situation changes drastically. Burgers-type equations of this type were proposed by one of us in [24] and later studied in [20, 17]. The novel feature of (1.6) is that large amplitude solutions develop discontinuities, while small solutions remain smooth at all times. This feature is easily demonstrated via the analysis of travelling waves [24, 20]: small amplitude kinks are smooth, while large amplitude kinks have embedded discontinuities (subshocks). Such subshocks may persist indefinitely since this is essentially a forced motion. Unlike the classical Burgers case, here, due to the saturation of fluxes, the viscous forces cannot counterbalance indefinitely inertial forces. Thus when the forcing exceeds a certain critical

threshold, discontinuity forms. In [24, 20], it was also demonstrated that both the continuous and discontinuous travelling waves are strong attractors for wide classes of appropriate initial data (for comprehensive analysis of (1.6) see [20, 17, 27]).

Embedding a saturating mechanism in the porous medium equation (1.4) leads to equation (1.1). For $n > 1$ this introduces both deep qualitative and quantitative changes, the most notable being a spontaneous formation of discontinuities out of continuous initial datum. In theorem 2.2 we prove the breakdown for compactly supported initial data. For strictly positive solutions, the shock discontinuity may also form, but only for 'large' initial datum. We illustrate this effect with a number of numerical experiments.

We would like to stress that there is a major difference between the formation of discontinuities in (1.1), which is a self-propelling effect, and the aforementioned convection–diffusion case (1.6), where the breakdown is enforced by the nonlinear convection. In the compactly supported case, one can intuitively explain the shock formation as an outcome of two competing mechanisms: on the one hand, the diffusion mechanism acts as to spread out the mass, on the other hand, the saturation 'freezes' the front causing the mass to 'pile-up' at the outer edges of the domain. This delays the motion of the front, which is one of the basic features of our model, until a jump discontinuity forms—then, and only then, the front begins to propagate.

We also study the large time behaviour of the patterns emerging out of the compactly supported data. Though the equation *per se* does not admit self-similar solutions, nevertheless the self-similar solutions of the corresponding model without saturation serve as attractors. We will demonstrate for $g(u) = u$ that away from the front vicinity the profiles converge asymptotically to their self-similar counterparts. Moreover, both the velocity of the front and the decay rate of the maximum of the solution approach the corresponding self-similar regimes.

We pause to comment upon the basic issue regarding the relations between the model's prediction and the reality it is supposed to describe. We argued that addition of flux saturation is a must to correct the divergence of the dissipation flux. As a consequence, we obtain a sharp discontinuity embedded in the pattern. In other words, we end up with a pattern which is even more singular than in the original nonsaturated model. How then, one may ask, is the reality better described by our model? This model advances our understanding in the sense that it makes us realize that, say, within a thermal wave in plasma, there will always be an internal layer where effects considered secondary, and thus neglected, become essential. The excessive amount of diffusion in the conventional model wherein the flux does not saturate, just smeared this effect. An analogy with gas dynamics may help to clarify the point: Euler equations predict formation of singularities, which could be avoided if instead one uses the Navier–Stokes equations. However, as is well known, viscosity only smears the discontinuity, while for its interior structure to be well described, one has to use kinetic theory. Even the width of the transition layer, unless the shock is weak, is not rendered properly by the Navier–Stokes equations. Thus, while our model cannot predict the interior structure of the discontinuity, which presumably will be very different for thermal waves or porous medium, it predicts the existence and the location of such a layer.

The cases of $g'(u) = u^{\pm 1}$ are also of notable interest. Without saturation the case $g'(u) = 1/u$ reduces for $n = 1$ to the linear heat equation. Here, if the initial datum is continuous, the solution remains continuous as well: no breakdown is possible. However, imposed initial discontinuities do not dissolve: they propagate, their amplitudes decrease and they persist indefinitely. This feature is demonstrated via a particular solution, which is self-similar in the vicinity of the shock front. The underlying ODE coincides with the equation corresponding to the self-similar solution constructed in [26] for equation (1.5), but the novelty of the presented case is that now it may take an infinite time to resolve the initial jump.

This paper is organized as follows. In section 2.1, we study equation (1.1) with $g(u) = u$ and $0 < n \leqslant 1$. The more interesting case $n > 1$ is studied in section 2.2, wherein the solution may lose its initial smoothness. The breakdown phenomenon is investigated in section 2.2.1. In section 2.2.2, we comment on the motion of the fronts. Asymptotic convergence towards the self-similarity of the standard porous medium equation (1.4) is discussed in section 2.3. The effect of 'delayed diffusion' for equation (1.1) with $g(u) = \ln u$ is studied in section 2.4. Concluding remarks can be found in section 3. The derivation of the studied models is presented in appendix A where the case $g'(u) = u$ is also discussed. In appendix B, numerical methods used in this paper are presented.

2. Equations with saturated dissipation fluxes

We first consider equation (1.1) with $g(u) = u$:

$$u_t = [u^n Q(u_x)]_x, \qquad n > 0. \tag{2.1}$$

Several other scenarios with different gs are discussed in sections 2.4 and appendix A. Notably, most of our results can be generalized for physically relevant choices of g. In all the numerical examples presented below, Q is chosen to be as in (1.2).

We assume that an initial datum,

$$u(x, 0) = u_0(x) \tag{2.2}$$

is non-negative, and in most of the cases we will consider compactly supported initial data.

We distinguish between two major cases: $0 < n \leqslant 1$ and $n > 1$. Let us start with the analysis of the simpler case.

2.1. $0 < n \leqslant 1$

We first try to establish an *a priori* bound on $|u_x|$. Differentiating (2.1) with respect to x, and denoting by $v := u_x$ results in

$$v_t = n(n-1)u^{n-2}Q(v)v^2 + nu^{n-1}Q(v)v_x + 2nu^{n-1}Q'(v)vv_x + u^nQ''(v)v_x^2 + u^nQ'(v)v_{xx}. \tag{2.3}$$

It is easy to see now that, for a smooth positive solution u, a positive maximum of v will decrease, while a negative minimum of v will increase in time since $\operatorname{sgn}[n(n-1)u^{n-2}] \leqslant 0$. This allows us to establish the following *a priori* bound:

$$\|u_x(\cdot, t)\|_{L^\infty} \leqslant \|u_0'(\cdot)\|_{L^\infty},$$

which guarantees that the solution preserve its initial smoothness if the initial datum is a positive smooth function (we omit the details of the proof, which is purely technical and rather straightforward).

If the initial datum is compactly supported the solution will behave similarly to the solution of the corresponding standard porous medium equation (1.4). Indeed, let us take $n = 1$ and the following initial datum,

$$u_0(x) = \begin{cases} \cos^4\left(\dfrac{\pi x}{2}\right), & \text{if } x \in [-1, 1], \\ 0, & \text{otherwise.} \end{cases} \tag{2.4}$$

The numerical solutions of the initial-value problems (IVPs) (2.1), (2.4) and (1.4), (2.4) are shown in figure 1. In both cases the fronts start moving as soon as u_x at the fronts becomes nonzero (the velocities of the fronts are equal to the corresponding values of $-Q(u_x)$).

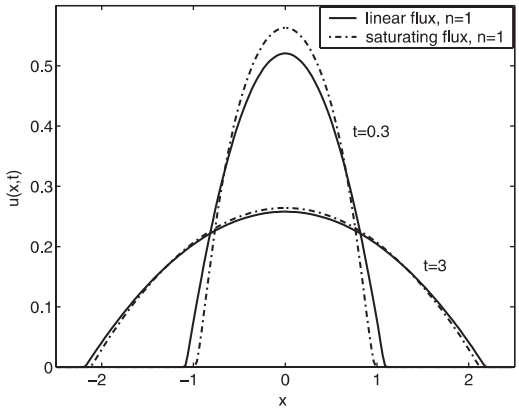

Figure 1. The solutions of the IVP (2.1), (2.4) and (1.4), (2.4) at times $t = 0.3$ and 3.

Actually, when $n < 1$ there is no qualitative difference between the cases of linear and saturated fluxes. The analysis for (2.1) is similar to the well-known analysis for (1.4) (see, e.g. [4, 5, 8, 10, 13, 18, 19]). That for $n < 1$ saturation has no impact is hardly surprising: near the front line, $x_f(t)$, the solution of (1.4) is proportional to $|x - x_f|^{1/n}$, and thus when $n < 1$, $u_x \sim 0$ and $Q \sim u_x$, which implies that the saturation mechanism is effectively shut off. The only possible exception to this scenario occurs if the initial datum is sharp at the edge, in which case the fronts start moving immediately and assumes a 'canonical' $|x - x_f|^{1/n}$ form.

2.2. $n > 1$

In this case, saturation of Q induces new effects. First, now even for positive initial data, solutions of equation (2.3) may not satisfy a maximum principle for $v \equiv u_x$, since $n(n-1) > 0$, and thus $\operatorname{sgn}[n(n-1)u^{n-2}Q(v)v^2] = \operatorname{sgn}(v)$. Consequently, a positive maximum of v may grow, and a negative minimum of v may decrease.

In the conventional, linear flux case, (1.4), $Q'(v) \equiv 1 \not\to 0$ as $|v| \to \infty$ which ensures that the solution remains continuous at all times. In this case, the competition between the first term on the right-hand side of (2.3), which stimulates breakdown of the solution, and the last term on the right-hand side is far more complex because large gradients may cause a loss of smoothness. Nevertheless, for smooth small initial data breakdown does not occur and the solution preserves its initial smoothness. The proof follows the arguments presented in [20] for the Burgers-type equation with saturated dissipation fluxes and, as stated in the following lemma, requires the uniform boundedness of u_x.

Lemma 2.1. *Let $u(x, t)$ be a classical positive solution of the IVP (2.1) and (2.2), and let $Q : \mathbb{R} \to (a, b)$, where $a < 0$ and $b > 0$. If the smooth initial datum is bounded away from zero,*

$$0 < m := \min_x u_0(x) \leqslant u_0(x) \leqslant \max_x u_0(x) =: M, \qquad \forall x, \tag{2.5}$$

and satisfies the following assumption,

$$\left(\frac{M}{m}\right)^n \|Q(u_0')\|_{L^\infty} \leqslant \alpha < \min(-a, b), \tag{2.6}$$

then for all $t \geqslant 0$

$$\|u_x\|_{L^\infty} \leqslant C.$$

Proof. First, we note that the solution of the (degenerate) parabolic equation (2.1) satisfies a maximum principle, which guarantees that

$$u(x,t) \geqslant m, \qquad \forall x, \forall t \geqslant 0. \tag{2.7}$$

We then rewrite equation (2.1) as

$$u_t = z_x, \tag{2.8}$$

where

$$z := u^n Q(u_x). \tag{2.9}$$

Differentiating (2.9) with respect to t and using (2.8), we obtain

$$z_t = nu^{n-1} Q(u_x) z_x + u^n Q'(u_x) z_{xx}. \tag{2.10}$$

Since $u > 0$ and $Q(u_x)$ is a bounded function satisfying $Q'(s) > 0\,\forall s$, equation (2.10) remains parabolic $\forall t > 0$, and its solution satisfies a maximum principle:

$$|u^n Q(u_x)| \leqslant |u_0^n Q(u_0')|, \qquad \forall t \geqslant 0. \tag{2.11}$$

We divide both sides of (2.11) by u^n, and then using the lower bound on u, (2.7), and the assumptions (2.5) and (2.6), we obtain

$$|Q(u_x)| \leqslant \alpha, \qquad \forall t \geqslant 0.$$

Due to the monotonicity of Q the last inequality implies that there exists a constant C such that $|u_x| \leqslant C$. This completes the proof of the lemma. □

Utilizing lemma 2.1 and following similar arguments to those found in [20] one obtains existence and uniqueness results (the proof is omitted).

Theorem 2.1 (existence and uniqueness of classical solutions). *Consider the IVP (2.1) and (2.2). Assume that the initial datum $u_0(x) \in C^3$ satisfies the assumptions (2.5) and (2.6). Then there exists a unique global classical solution of (2.1) and (2.2), $u(x,t) \in C^{2,1}(x,t)$.*

Remark. The assumption (2.6) means that theorem 2.1 guarantees smoothness of the positive solution only if the initial gradients and the ratio $\max_x u_0(x)/\min_x u_0(x)$ are small. We note that in the case of the standard porous medium, positive solutions cannot lose their initial regularity. Moreover, if the positive initial datum is not smooth, it will be immediately smoothed out as in the case of the conventional, linear flux, heat equation. When Q is bounded, the situation is not as simple and the solution may lose its initial smoothness. To illustrate this phenomenon consider a 'small',

$$u(x,0) = -0.5\cos(0.5\pi x) + 0.6 \tag{2.12}$$

and 'large',

$$u(x,0) = -5.0\cos(0.5\pi x) + 5.5, \tag{2.13}$$

infinitely smooth periodic initial data. We take $n = 2$, and compute the solutions of the IVPs (2.1), (2.12) and (2.1), (2.13). As one can see in figure 2, the solution remains smooth in the first case yet it breaks down in the second case when the initial datum is large.

The observed breakdown of initially smooth positive solutions can be attributed to the impact of saturated diffusion flux. Though we could not prove breakdown of positive solutions, our numerical results (figure 2) clearly demonstrate that if the assumption (2.6) is not satisfied, positive solutions of the IVP (2.1) and (2.2) may develop spontaneous discontinuities.

We note that it was proved in [12, theorem 2.3], that the solution of (2.1) may break down if the smooth positive initial datum is an increasing function. In the next section, we will prove that for a compactly supported solution that remains smooth inside its support, sharp fronts form in a finite time. However, it is still an open problem how to prove the breakdown for more general cases.

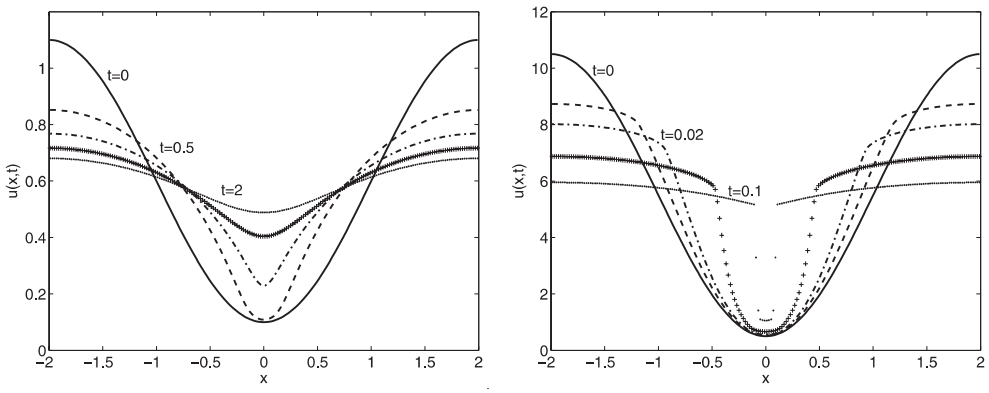

Figure 2. The solutions of (2.1) with the 'small', (2.12), and 'large', (2.13), initial data, $n = 2$.

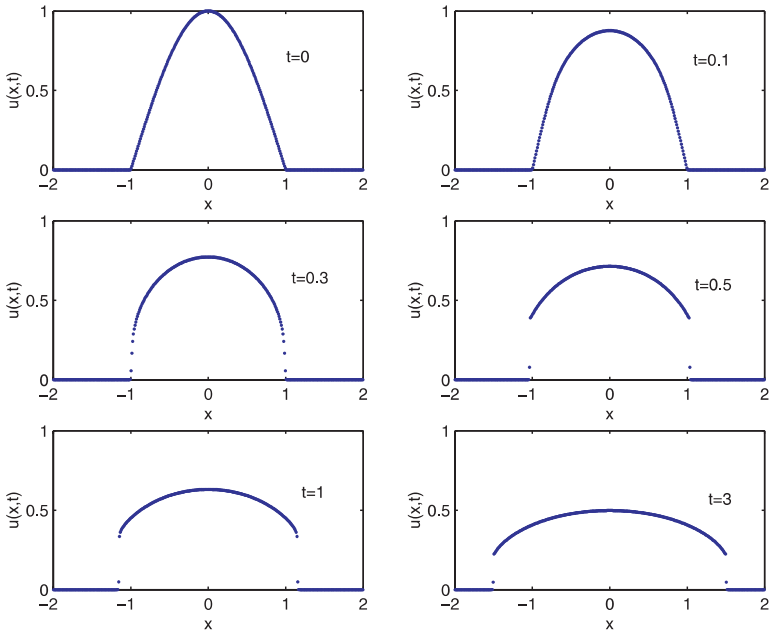

Figure 3. The solution of (2.1) and (2.14) with $n = 2$.

2.2.1. Breakdown. We now consider equation (2.1) with $n > 1$, subject to continuous compactly supported initial data. As a first example we set (see figure 3),

$$u_0(x) = \begin{cases} \cos\left(\dfrac{\pi x}{2}\right), & \text{if } x \in [-1, 1], \\ 0, & \text{otherwise.} \end{cases} \tag{2.14}$$

Snapshots of the numerical solution of (2.1), (2.14) and $n = 2$, are shown in figure 3 and reveal that initially, though the profile of the pulse changes, it remains continuous and confined to its initial support that does not change. However, at $t = 0.5$ one can observe that the profile has developed a sharp discontinuity at each side, and the fronts have started moving.

Let us now determine the speed of the front. To this end we assume that the initial datum (2.2) is compactly supported, and denote by $x_f(t)$ the location of the right end of the

support at time t. We also define

$$F(x_{\rm f}(t),t) := \int_{-\infty}^{x_{\rm f}(t)} u(\xi,t)\,{\rm d}\xi$$

and differentiate it with respect to t. We then obtain

$$\frac{\rm d}{{\rm d}t}F(x_{\rm f}(t),t) = F_x(x_{\rm f}(t),t)\dot{x}_{\rm f}(t) + F_t(x_{\rm f}(t),t) = u_{\rm f}\dot{x}_{\rm f}(t) + \int_{-\infty}^{x_{\rm f}(t)} u_t(\xi,t)\,{\rm d}\xi, \tag{2.15}$$

where $\dot{x}_{\rm f} \equiv {\rm d}x_{\rm f}(t)/{\rm d}t$ and $u_{\rm f} := u(x_{\rm f}(t)-0,t)$. Using equation (2.1), we compute

$$\int_{-\infty}^{x_{\rm f}(t)} u_t(\xi,t)\,{\rm d}\xi = \int_{-\infty}^{x_{\rm f}(t)} [u^n(\xi,t)Q(u_x(\xi,t))]_\xi\,{\rm d}\xi = u^n Q(u_x)|_{x=x_{\rm f}-0}. \tag{2.16}$$

Since

$$\int_{-\infty}^{x_{\rm f}(t)} u(\xi,t)\,{\rm d}\xi = \int_{-\infty}^{\infty} u(\xi,t)\,{\rm d}\xi,$$

the left-hand side of (2.15) is $({\rm d}/{\rm d}t)F(x_{\rm f}(t),t) = 0$, and therefore, substituting (2.16) into (2.15) results in

$$u_{\rm f}\dot{x}_{\rm f}(t) = -u^n Q(u_x)|_{x=x_{\rm f}-0}. \tag{2.17}$$

Dividing both sides by $u_{\rm f}$, we obtain the following formula for the speed of the front:

$$\dot{x}_{\rm f}(t) = -u^{n-1} Q(u_x)|_{x=x_{\rm f}-0}. \tag{2.18}$$

Remarks.

(1) The same procedure is used to find the speed of the left front, but the auxiliary function is now:

$$F(x_{\rm f}(t),t) := \int_{x_{\rm f}(t)}^{\infty} u(\xi,t)\,{\rm d}\xi.$$

(2) If the front is discontinuous, the front speed can be also computed using the Rankine–Hugoniot condition, which says that for the hyperbolic conservation law, $u_t + f(u)_x = 0$, the shock speed is

$$s = \frac{f(u_{\rm l}) - f(u_{\rm r})}{u_{\rm l} - u_{\rm r}}, \tag{2.19}$$

where $u_{\rm l}$ ($u_{\rm r}$) is the value of the solution on the (2.24) and (2.14), left (right) side of the shock. One may (formally) view equation (2.1) as a conservation law with $f = -u^n Q(u_x)$, and thus according to (2.19) the front speed is

$$s = \dot{x}_{\rm f}(t) = \frac{-u^n(x_{\rm f}-0,t)Q(u_x(x_{\rm f}-0,t))+0}{u(x_{\rm f}-0,t)-0} = -u^{n-1}Q(u_x)|_{x=x_{\rm f}-0}. \tag{2.20}$$

(3) If $u_{\rm f} = 0$, the division by $u_{\rm f}$ in (2.17) may be avoided if we approximate the solution inside its support by adding a small constant $\varepsilon > 0$. Then $u_{\rm f}$ equals to ε and we may divide (2.17) by $u_{\rm f}$. Passing to the limit in (2.18) as $\varepsilon \to 0$, we obtain $\dot{x}_{\rm f}(t) = 0$, since $Q(u_x)$ is bounded for any value of u_x.

(4) We would like to mention that a similar jump condition for equation (1.3) with strictly convex $\varphi(u)$ and an increasing initial datum was obtained in [12]. However, in this case the left and the right limits of u_x became infinite on the jump and therefore the corresponding limits of $Q(u_x)$ are both equal to $Q_\infty := \lim_{s\to\infty} Q(s)$. Note that in our problem numerical experiments clearly indicate that both the left and the right limits of u_x are finite (see, e.g. figures 2, 3, 6 and 7).

Unlike the standard porous medium case, (1.4), wherein $Q(u_x) = u_x$ is unbounded in u_x, the fronts of the solution of (2.1) and (2.2) will stay put as long as the compactly supported solution remains continuous. Concurrently, within the inner parts of the pulse the diffusion 'pushes' the mass outward. This leads to sharpening of the gradients and eventually to the formation of jump discontinuities. This property is expressed in the following theorem.

Theorem 2.2 (breakdown of compactly supported solutions). *Consider equation (2.1) with $n > 1$ subject to a compactly supported, smooth, non-negative initial datum (2.2). In addition, assume that $u_0(x)$ is an even concave function. Suppose that $u(x, t)$ is a compactly supported weak solution of (2.1) and (2.2), which remains $C^{3,1}(x, t)$-smooth inside its support, $(-x_f(t), x_f(t))$, for all $t \geqslant 0$. Then there exists a finite time $T^* > 0$ such that $u(x, T^*)$ has jump discontinuities at $x = \pm x_f(T^*)$.*

Proof. First, we note that it is easy to show that the solution of (2.1) and (2.2) preserves its initial structure, i.e. it remains even and concave (the proof is left to the reader). Then, as in the proof of lemma 2.1, we consider the function $z := u^n Q(u_x)$, which satisfies the (degenerate) parabolic equation (2.10). Let $\tilde{x}(t) > 0$ be a point of minimum of z, then it follows from (2.10) that

$$\dot{\tilde{x}}(t) = -nu^{n-1} Q(u_x)|_{x=\tilde{x}(t)}, \tag{2.21}$$

where $\dot{\tilde{x}} = \mathrm{d}\tilde{x}/\mathrm{d}t$. Note that $z(\tilde{x}(t), t)$ is negative, and hence $\dot{\tilde{x}}(t) > 0$ for all $t \geqslant 0$.

Let us assume that the solution of (2.1) and (2.2) remains continuous for all $t \geqslant 0$. Then, as we have shown before, the front does not move, i.e. $x_f(t) \equiv x_f(0)$, and the minimum of z must stay on the left of $x_f(0)$, i.e. $\tilde{x}(t)$ must be smaller than $x_f(0)$ for all $t \geqslant 0$, since $z(x, t) = 0$ for $x \geqslant x_f(0)$. Therefore there exists a subsequence $\{t_k\} \to \infty$ such that $\lim_{t_k \to \infty} \dot{\tilde{x}}(t_k) = 0$, and hence $\forall \varepsilon < 0$ there exists a finite time T such that

$$\dot{\tilde{x}}(T) = -nu^{n-1} Q(u_x)|_{x=\tilde{x}(T)} < \varepsilon.$$

Since u is a bounded positive function, it follows from the last inequality that

$$z(\tilde{x}(T), T) > \varepsilon_1 := -\frac{\varepsilon}{n} \|u\|_{L^\infty}. \tag{2.22}$$

Let us now denote by $\bar{u}$ the mean value of u, i.e.

$$\bar{u} := \frac{1}{x_f(t)} \int_0^{x_f(t)} u(x, t)\, \mathrm{d}x \equiv \frac{1}{x_f(0)} \int_0^{x_f(0)} u_0(x)\, \mathrm{d}x.$$

Obviously, there exists a point $x = \delta \in (0, x_f(0))$ such that $u(\delta, T) = \bar{u}/2$. Since $u(x, T)$ is concave, we can estimate its derivative as follows (see figure 4),

$$u_x(\delta, T) \leqslant \frac{u(\delta, T) - u(0, T)}{\delta - 0} < \frac{(1/2)\bar{u} - \bar{u}}{x_f(0)} = -\frac{\bar{u}}{2x_f(0)}.$$

Using the last inequality and the fact that $u^n(\delta, T) = \bar{u}^n/2^n$, we obtain

$$z(\delta, T) = \frac{\bar{u}^n}{2^n}\, Q\left(-\frac{\bar{u}}{2x_f(0)}\right),$$

which is smaller than ε_1 provided ε is sufficiently small. This contradicts the estimate (2.22). Therefore, there exists a final time T^* such that $\tilde{x}(T^*) = x_f(T^*)$, and hence the solution $u(x, T^*)$ must become discontinuous at $x = x_f(T^*)$. Symmetry implies that it is also discontinuous at $x = -x_f(T^*)$. This concludes the proof of theorem 2.2. □

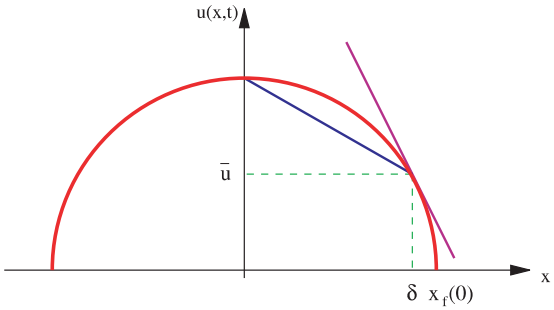

Figure 4. Illustration to the proof of theorem 2.2.

Remark. The presented proof does not provide any information as to the time of the breakdown and the height of the jump. The size of the jump may be estimated using the following argument: let D be the size of the initial support and let $M = \int_{-\infty}^{\infty} u_0(x)\,\mathrm{d}x$ be the total 'mass' of the process which, of course, is conserved. If the motion of the front was delayed until the whole pulse becomes a rectangle, then M/D is the size of the height. Though for a typical convex data this is a fair estimate, for compact data with long 'tails', and thus large D, this is a poor estimate. It is also too rough when a breakdown occurs inside the support (see figures 6 and 7).

2.2.2. Remarks on the motion of the fronts. In order to understand how motion of the front is delayed, it is necessary to return to the mechanism of delay in the classical linear flux case, which was extensively studied in [6, 7]. First of all, we recall that having a finite speed of front propagation is a consequence of the degeneracy of the parabolic equation at $u = 0$. Now, given an initial datum such that $u_0(x) = 0$ for $x \geqslant 0$, the subsequent evolution will depend on the slope of u near the front line. According to [6], if $u \sim |x|^{\alpha}$ near the front line, then $\alpha_* := 2/n$ will be a critical value in the sense that there will be a delay in the propagation of initial datum if the front line is 'under' the 'waiting parabola' $|x|^{2/n}$, i.e. $\alpha > \alpha_*$, otherwise the front starts moving immediately. If the initial datum is completely under the 'waiting parabola', the waiting time is a universal quantity which depends only on n. If, on the other hand, it is under the 'waiting parabola' only locally, then the waiting time depends on global features like the distribution of the mass within the pulse. In any case, once the front starts moving the slope of the front is given by $u \sim |x - x_{\mathrm{f}}|^{1/n}$.

Returning to our problem with saturation, we first distinguish the value of $\alpha = 1$. If $\alpha > 1$, at least initially, the saturating mechanism should be ineffective on the front. On the other hand, if $\alpha < 1$ it intervenes immediately, which means that the front and its vicinity are dominated at once by the saturation mechanism. Note, however, that this does not imply immediate movement of the front. In fact, though at the front line Q degenerates, elsewhere the equation remains parabolic, and only after a discontinuity forms at the front line will it start moving. As it can be seen from the variety of the numerical examples to be presented, the moment at which the motion begins is not a universal quantity, and to a large extent it is determined by the particulars of the mass distribution.

For $\alpha \geqslant 1$ there are two possible scenarios.

($\mathcal{A}$) $\alpha < \alpha_*$, which may occur if $1 < n \leqslant 2$. Since $\alpha \geqslant 1$, gradients vanish on the front which should deactivate the saturation. But now, since $\alpha < \alpha_*$, the results for the classical linear flux case imply that the corresponding classical front should form and move right away. Yet, if this occurs then on the front $u \sim |x - x_{\mathrm{f}}|^{1/n}$ which, for $n > 1$, would imply the

divergence of u_x. However, this in turn evokes the saturation mechanism into action which halts the motion until a jump forms. Thus, in this case, the classical mechanism at the front acts to cause its own demise.

($\mathcal{B}$) $\alpha \geqslant \alpha_*$. Now not only the saturation mechanism is suppressed but, since the pulse is under the 'waiting parabola', the front line actually waits in a classical linear flux manner. This waiting will be ultimately disrupted by a shock that forms inside. The formation of the shock is a 'geometrical' effect. The large diffusion at the centre pushes the mass outside, while at the outer parts, due to the very small values of u, diffusion is so small that there is hardly any dynamics. Therefore there is a rapid transition from one regime into the other which, with the 'help' of saturated diffusion activated by sharp gradients, turns into a sharp jump. This jump travels toward the awaiting front line which starts moving upon its arrival. This scenario can be clearly observed in figure 6 (here $\alpha = 1, n = 3$, and thus $\alpha_* = \frac{2}{3}$). For small times the solution of this case is similar to the solution of the $n = 2$ case (figure 3). Yet, at $t = 0.5$ one can observe sharp discontinuities inside the support for $n = 3$. After their formation the discontinuities propagate, and at larger times ($t = 1, 3$) the solutions in both cases, apart from the natural differences between the various ns, look very similar.

In all examples considered so far we have assumed that the initial datum is continuous. However, jump-condition (2.20) implies that if the front is initially discontinuous, the motion will begin at once. This is a purely kinematic effect caused by the jump and has very little to do with the 'mature' jump, which develops during the evolution and reflects the total mass of the system. In figure 5, we display near the front the response to the initial perturbation of (2.14),

$$u = \begin{cases} \dfrac{\sigma \cos(\sigma x)}{2 \sin \sigma}, \quad \sigma := \dfrac{\pi}{2+k}, & \text{if } x \in [-1, 1], \\ 0, & \text{otherwise}, \end{cases} \tag{2.23}$$

for $k = 0, 0.02$, and $k = 0.1$ and $t = 0, 0.1, 0.3, 0.5$. The normalization used assures that all pulses have the same mass. One clearly observes the effect due to the initial jump which at $t = 0.1$ is hardly noticeable for $k = 0.02$, but quite evident for $k = 0.1$. For $t = 0.3$ the behaviour on the front still reflects the initialization, but at $t = 0.5$, the jump is pretty much the same for all cases, which reflects a global effect: the same mass in each case.

In theorem 2.2, we have assumed that the solution remains smooth inside its support for all $t > 0$. However, as we have explained in case ($\mathcal{B}$) above, this assumption, which obviously is true for the classical linear flux case, may not be satisfied in our problem since the solution may break down inside the support. Another numerical example which illustrates a breakdown inside the support is obtained upon taking $n = 2$, but with the C_0^3 initial datum (2.4), compare figures 7 and 6. Now $\alpha_* = 1$, but $\alpha = 4$, which clearly belongs to case ($\mathcal{B}$). It is also instructive to see how in the linear flux case same initial pulse evolves (see figure 8). Here the front is delayed by the same classical effect but, of course, no shock within the domain is possible.

It is also instructive to follow the evolution of a variety of initial pulses, all having the same 'mass'. We thus consider equation (2.1) subject to the following initial data:

$$u_0(x) = \begin{cases} \cos^2\left(\dfrac{\pi x}{2}\right), & \text{if } x \in [-1, 1], \\ 0, & \text{otherwise}, \end{cases} \tag{2.24}$$

$$u_0(x) = \begin{cases} \sin^2(\pi x), & \text{if } x \in [-1, 1], \\ 0, & \text{otherwise}. \end{cases} \tag{2.25}$$

The total 'mass' in all the cases is identical and equal to 1. The evolution from $t = 0$ until $t = 1.5$ is shown in figures 9 and 10.

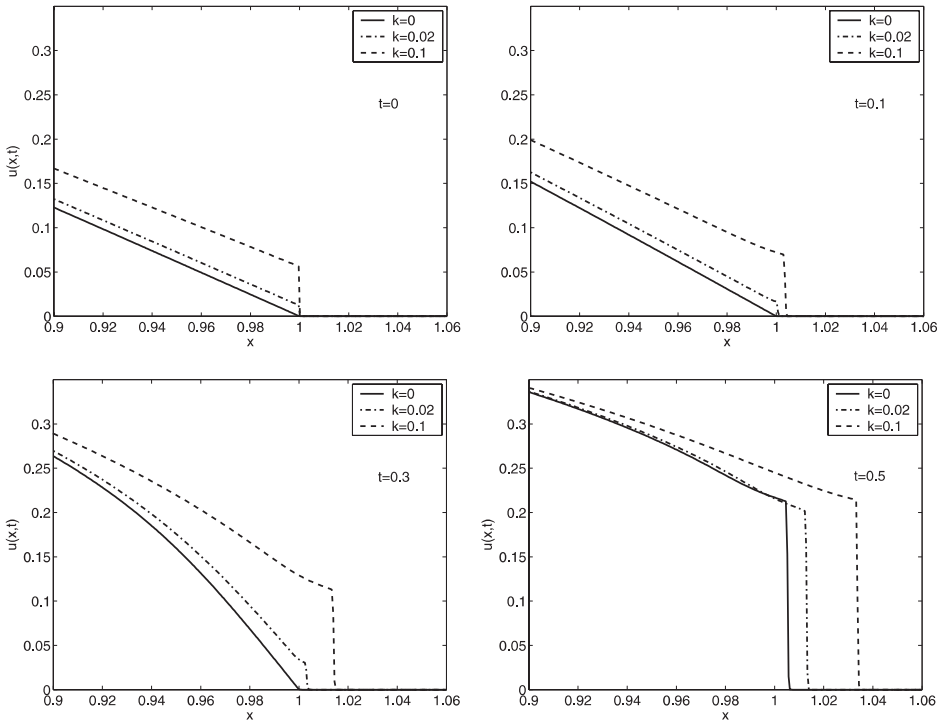

Figure 5. Comparison of the behaviour of the solutions of (2.1) and (2.23) with $n = 2$ in the vicinity of the initially continuous ($k = 0$) and discontinuous ($k = 0.02, 0.1$) fronts.

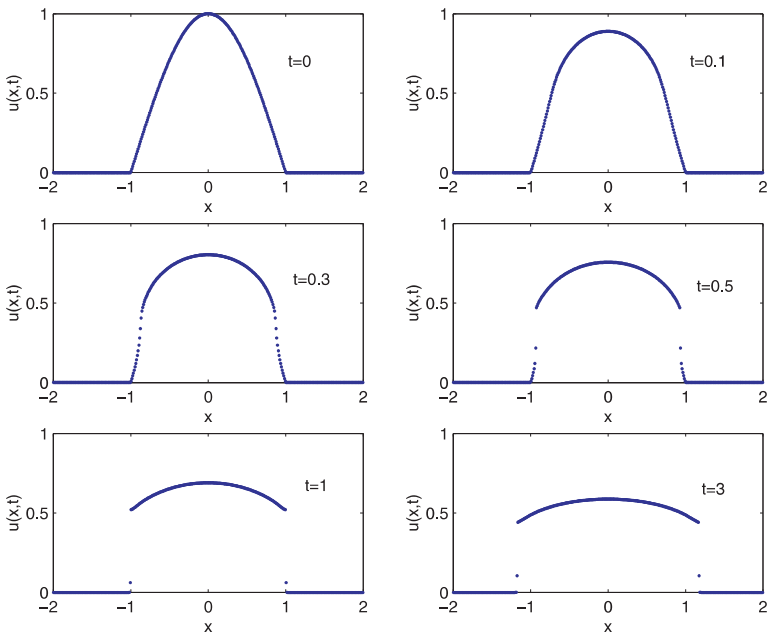

Figure 6. The solution of (2.1) and (2.14) with $n = 3$.

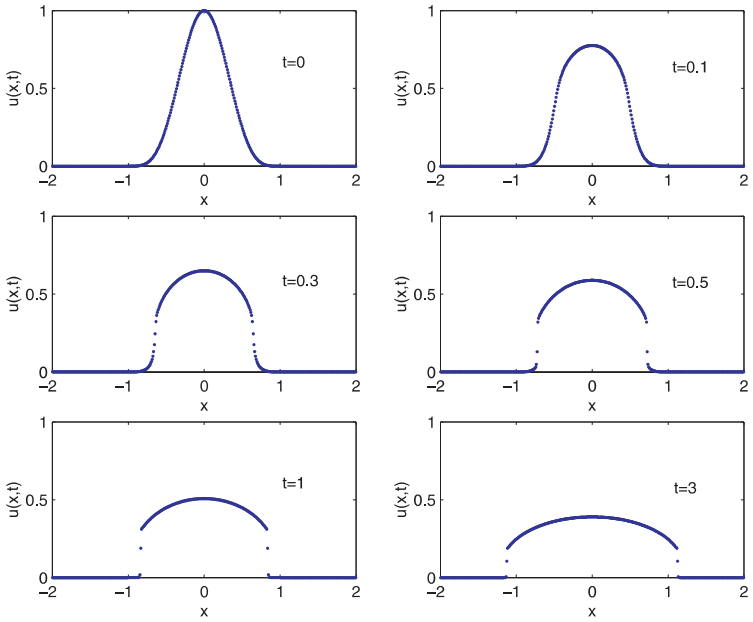

Figure 7. The solution of (2.1) and (2.4) with $n = 2$.

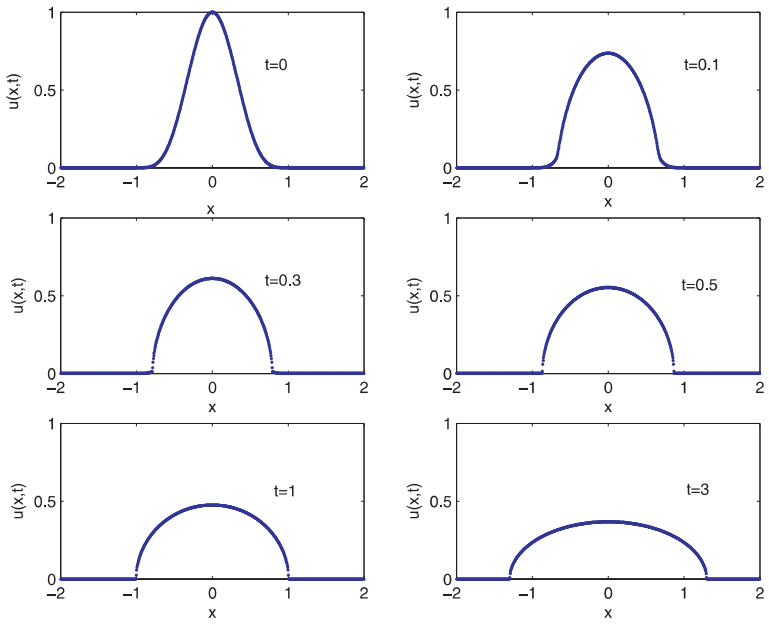

Figure 8. The solution of (1.4) and (2.4) with $n = 2$.

The most notable effect can be seen in figure 10: until $t = 0.3$, each half of the pulse is disconnected from the other, and the centre of mass of each part is closer to the front than in all other examples. The shocks which form in each domain have smaller distances to traverse, therefore the support starts moving in an earlier time than in all other examples.

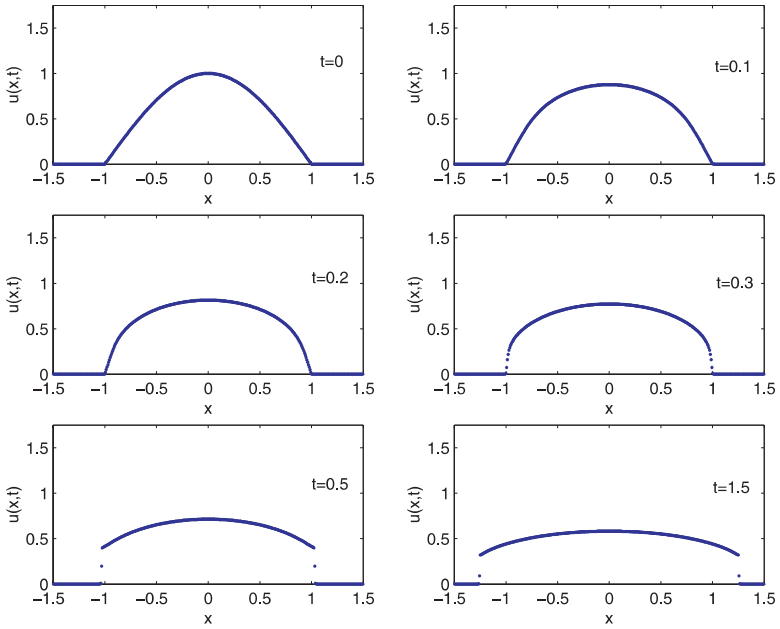

Figure 9. The solution of (2.1) and (2.24) with $n = 2$.

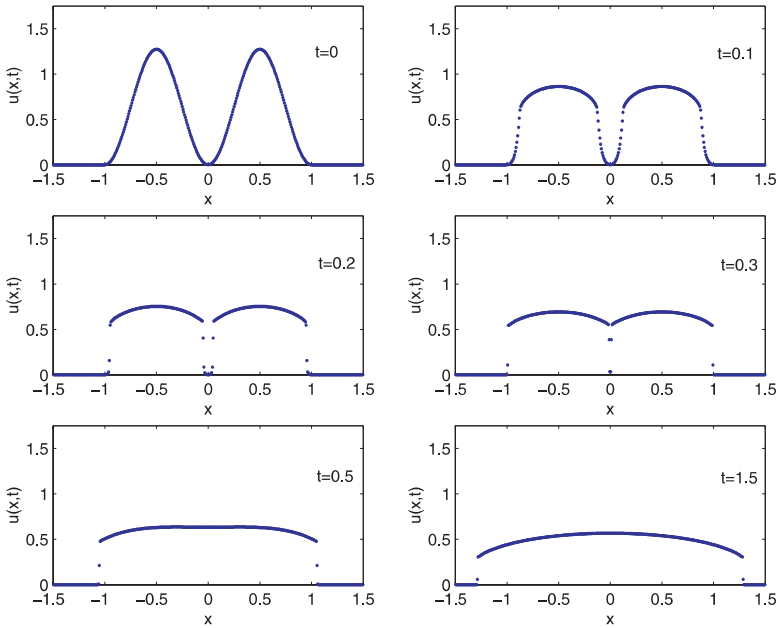

Figure 10. The solution of (2.1) and (2.25) with $n = 2$.

2.3. Convergence to the self-similar regime

In this section, we examine numerically the emergence of an intermediate stage of evolution wherein the initial conditions have been 'washed out', but the process is still far enough from

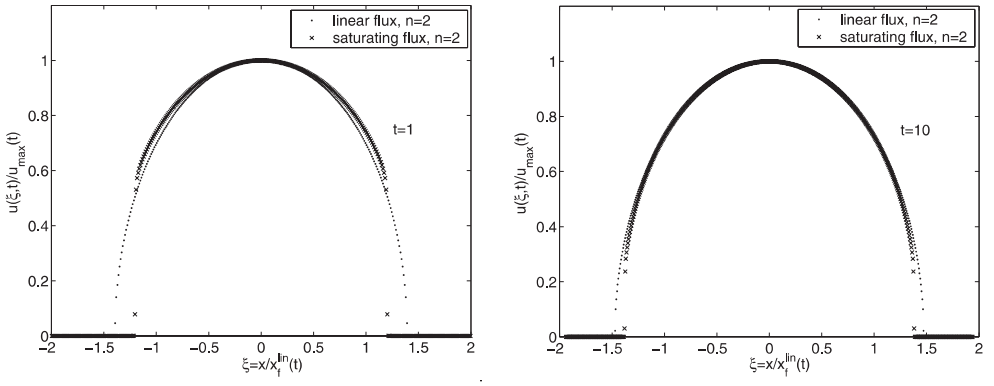

Figure 11. Comparison of the solutions of (1.4), (2.14) and (2.1), (2.14) with $n = 2$, plotted in normalized amplitudes. $u_{\max}^{\mathrm{lin}} \approx 0.61$, $u_{\max}^{\mathrm{sat}} \approx 0.63$ at $t = 1$, and $u_{\max}^{\mathrm{lin}} \approx 0.36$, $u_{\max}^{\mathrm{sat}} \approx 0.37$ at $t = 10$.

its 'ultimate death'. In figure 11, we compare the evolution of the classical porous medium case ($n = 2$) with its saturating counterpart. The scaled coordinate ξ is equal to $x/x_{\mathrm{f}}^{\mathrm{lin}}(t)$, where $x_{\mathrm{f}}^{\mathrm{lin}}(t)$ is the location of the front of classical self-similar solution and, once the total initial mass is given, it can be calculated explicitly (see, e.g. [28]).

To demonstrate the convergence of the saturated flux process to the conventional one, we normalize the maximal amplitudes of both profiles to 1. The results are shown in figure 11. Note that since $\int_{-\infty}^{\infty} u \, \mathrm{d}x$ is conserved, the delayed position of the front, when compared with the linear flux case, results in a higher peak at the centre. As time advances one observes an increasing spread of an overlap, starting from the centre and moving out, with both pulses being 'united in death'.

In figure 12, the convergence is investigated more quantitatively. Since in its self-similar stage the solution of the linear flux case has the form

$$u \sim t^{-1/(n+2)} f(\zeta), \qquad \text{where } f(\xi) = [1 - \zeta^2]^{1/n}, \quad \zeta \sim x t^{-1/(n+2)}, \tag{2.26}$$

it is natural to compare the rate of the decay of both pulses and the location of their fronts in logarithmic units. From (2.26) we obtain a linear relation between $\ln u_{\max}(t)(\ln x_{\mathrm{f}}(t))$ and $\ln t$ with the slope $\mp 1/(n+2)$, respectively. The convergence can be clearly seen. From numerical simulations it has been found that when $n = 2$, the slope of the dotted line in figure 12 is equal to 0.26 for the front $x_{\mathrm{f}}(t)$, and -0.25 for the maximum of the solution $u_{\max}(t)$. When $n = 3$, the slope of the dotted line is equal to 0.22 for the front $x_{\mathrm{f}}(t)$, and -0.21 for the maximum of the solution $u_{\max}(t)$. The numerical values agree quite well with the analytical values predicted by (2.26). One may also note the considerable waiting times (until the shock forms) of the saturating process. This delay is then compensated by an accelerated 'catch-up' motion.

Remark. For the standard porous medium case, given a class of initial data $u_0(x)$, insofar that they all have the same 'mass', $\int_{-\infty}^{\infty} u_0(x) \, \mathrm{d}x$, their asymptotic stage is identical, with differences in initial distribution being 'washed away' very quickly. In the saturated case, the onset of motion depends on the details of initial distribution, and therefore the location of the front at a given time is not a universal quantity, but carries a memory of the initialization. At a late phase of evolution we expect those differences to diminish similarly to the linear flux case. This can be observed by looking at the examples at the end of section 2.2.2. In figure 13, the solutions at a large time ($t = 20$) of the two very different initializations are presented. Clearly, at $t = 20$ the solutions approach the same asymptotic stage.

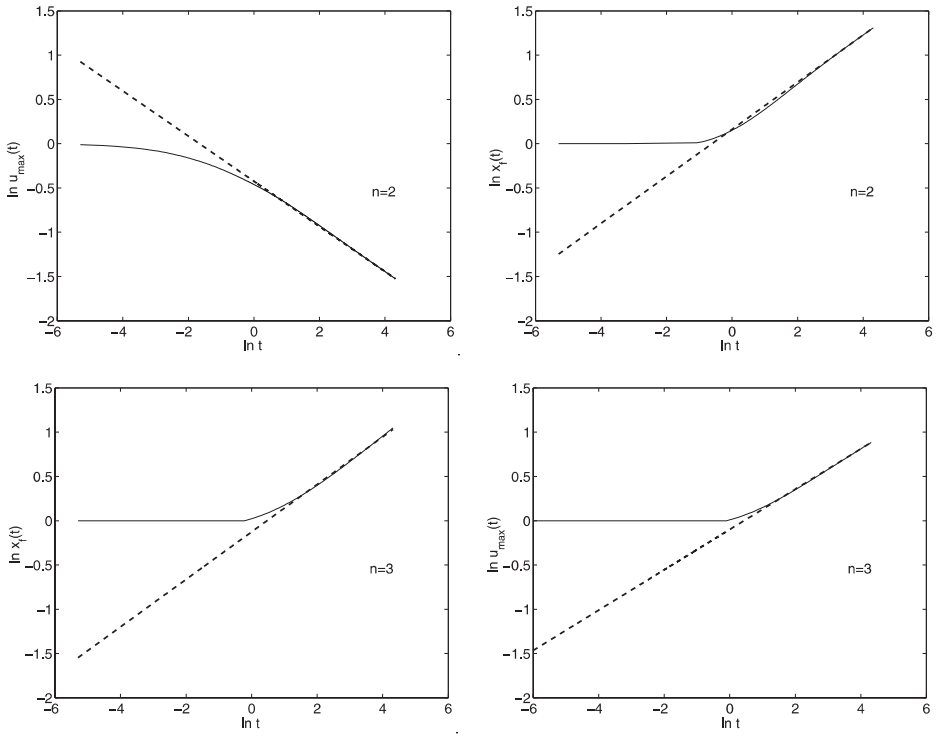

Figure 12. Asymptotic convergence of the fronts (left) and decay rate of the amplitudes (right) for (2.1) and (2.14) ($n = 2$ and 3) to the corresponding quantities in the linear flux case.

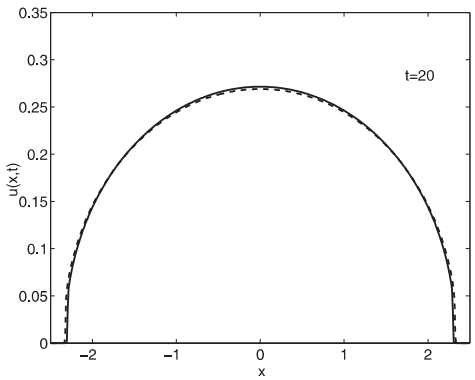

Figure 13. Convergence of two solutions of (2.1) with $n = 2$ and the initial conditions (2.24) and (2.25) to the same asymptotic state.

2.4. An alternative saturation mechanism: $g'(u) = 1/u$

In this section, we consider equation (1.1) with $g(u) = \ln u$, [23], namely,

$$u_t = [u^n Q((\ln u)_x)]_x, \tag{2.27}$$

where we set $g(u)_x := 0$ if $u = 0$. Compared with (2.1), this equation has several additional features. For instance, it is invariant under the transformation $u \to Au, x \to x, t \to A^{n-1}t$,

which implies that exactly as in the linear flux case, stretching the amplitude by a factor of A stretches the time units by a factor of A^n.

If $n > 1$ the solution of (2.27) behaves similarly to the corresponding solution of (2.1), where $g(u) = u$. To cite an example, in figures 14 and 15, we show the solution of the IVP (2.27) and (2.14) with $n = 3$. One can note not only the increased delay in propagation, but also the fact that the pulses flatten out with time, and do not seem to converge to their linear flux counterparts. This effect is demonstrated in figure 15 (right), where the location of the right fronts and the amplitudes of the solutions at different times are normalized to 1. Clearly, they do not converge to a definite pattern. This feature appears to be generic to all cases wherein $g'(u)$ is a decreasing function. In such cases, the saturating part has a more

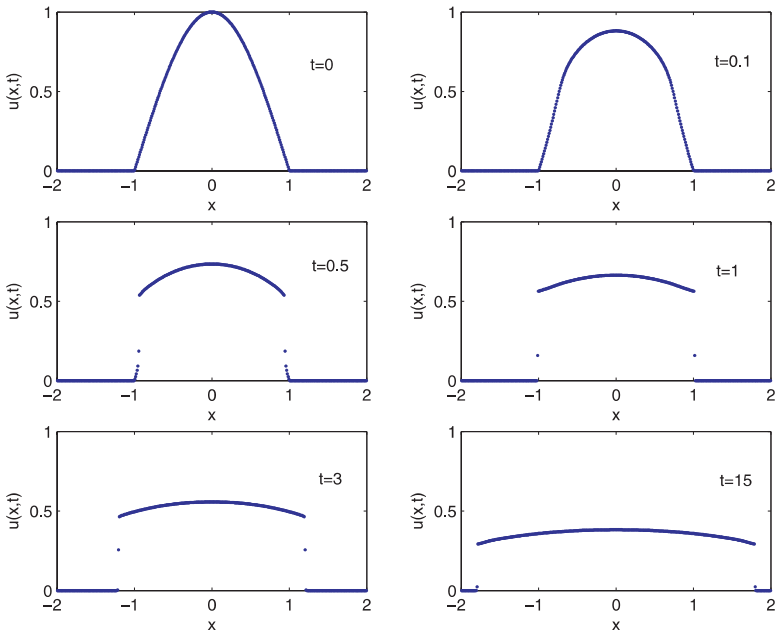

Figure 14. The solution of (2.27) and (2.14) with $n = 3$.

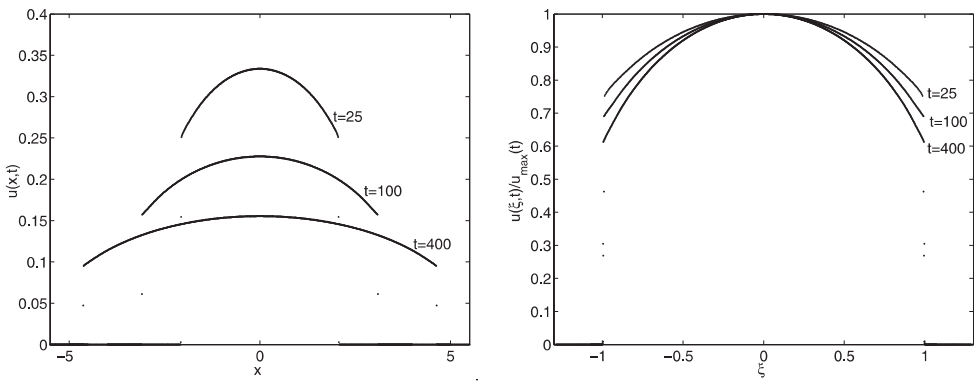

Figure 15. The solution of (2.27) and (2.14) with $n = 3$ in the original (left) and normalized (right) coordinates. Note that unlike the previous cases, the profiles do not approach a universal shape.

pronounced effect in the outer parts of the pulse, resulting in an almost isothermal distribution of the pulse, followed by a sharp drop at the centre. Figure 15 (left) provides an idea of the extent to which the present saturation process slows the expansion.

Though the profiles do not converge to the corresponding self-similar linear flux profiles, nevertheless both the velocity of the front and the rate of decay do converge to an asymptotic limit. As one can see in figure 16, in the asymptotic limit, the front propagates at the same rate as in the linear flux case. However, the rate of amplitude decay at the centre, though close, is different in both cases: compare the slopes for $n = 2$ in figure 12 with the slopes in figure 16.

In the remainder of this section, we will consider the $n = 1$ case. We assume that Q is an increasing bounded function, such that $Q(s) = -Q(-s)\ \forall s$, $Q'(s) \sim K|s|^{-\beta}$ as $|s| \to \infty$; $\beta > 2$, $K > 0$ are constants, and let the initial datum be the step function

$$u_0(x) = \begin{cases} U_0 \equiv \text{const.} > 0, & \text{if } x < 0, \\ 0, & \text{if } x > 0. \end{cases} \tag{2.28}$$

We now study the evolution of this datum. First, we note that the initial discontinuity will propagate to the right, and that the size of the jump will decrease in time. It is not clear though whether the solution will be smoothed out, and if so, whether it will occur in a finite time. In figure 17 (left), the numerical solution of the IVP (2.27) and (2.28) with $U_0 = 1$ is plotted at times $t = 0.1, 1$. Though the resolution achieved by the numerical method described

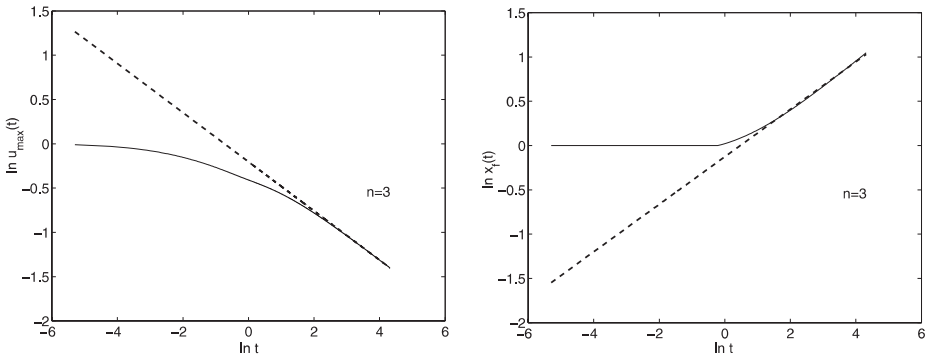

Figure 16. Asymptotic convergence of the front (left) and decay rate of the amplitude (right) for (2.27) and (2.14) ($n = 3$) to the corresponding quantities in the linear flux case.

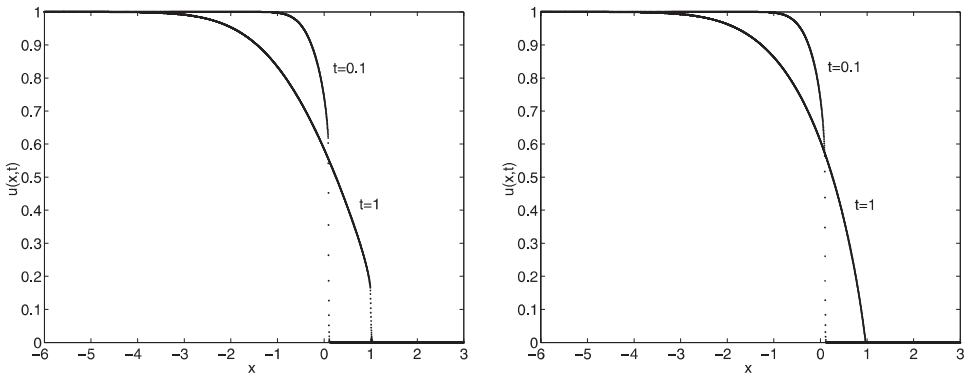

Figure 17. The solutions of (2.27), (2.28) (left) and (2.1), (2.28) (right) with $n = 1$ and $U_0 = 1$ at $t = 0.1$ and 1.

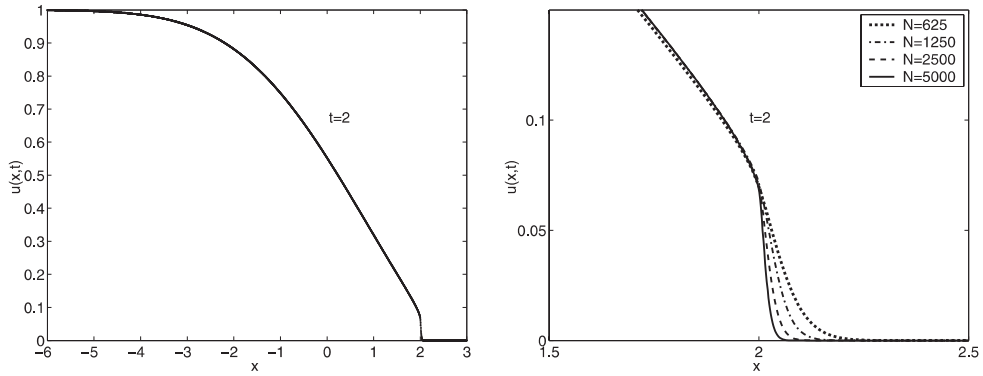

Figure 18. The solution of (2.27) and (2.28) with $U_0 = 1$ at $t = 2$. The picture on the right focuses on the solution near the front, computed with a different number of grid points.

in appendix B is not very good, one can observe the presence of the shock discontinuity on the front. The difficulty in capturing the shock is more pronounced at large times, since the amplitude of the shock decreases. The computed solution of the same IVP at $t = 2$ shown in figure 18 illustrates this effect. The numerical shock layer has many points, but when with the increase of the number of grid points, the front significantly sharpens. This supports our conjecture that the discontinuity will not disappear within finite time.

Remark. Note that contrary to the saturation mechanism studied in this section, the corresponding solutions of equation (2.1) with $n = 1$ will sustain an initially imposed discontinuity for a finite time only. The difference between the two cases can be clearly seen in figure 17.

In the remaining part of this section, we will construct a particular solution of the IVP (2.27) and (2.28), which is discontinuous for any finite time. To this end, we consider a slightly modified initial datum:

$$u_0(x) = \begin{cases} U_0 \equiv \text{const.} > 0, & \text{if } x < 0, \\ \varepsilon, & \text{if } x > 0, \end{cases} \tag{2.29}$$

where $\varepsilon \ll U_0$ is a small positive constant. We seek a solution of the IVP (2.27) and (2.29) in the following self-similar form:

$$u(x,t) = \begin{cases} U_0\, \mathrm{e}^{-h(\xi)\sqrt{t}}, & \text{if } x < x_\mathrm{f}(t), \\ \varepsilon, & \text{if } x > x_\mathrm{f}(t), \end{cases} \tag{2.30}$$

where the similarity variable is

$$\xi := \frac{x - x_\mathrm{f}(t)}{\sqrt{t}} \tag{2.31}$$

and $x_\mathrm{f}(t)$ is the location of the jump discontinuity at time t ($x_\mathrm{f}(0) = 0$). Notice that the interval $x < x_\mathrm{f}(t)$ ($x > x_\mathrm{f}(t)$) corresponds to the interval $\xi < 0$ ($\xi > 0$), and that $\xi = 0$ at the shock front.

Substituting (2.30) into (2.27), we obtain the following equation for the function $h(\xi)$ in the interval $\xi < 0$:

$$\tfrac{1}{2}(h'(\xi)\xi - h(\xi)) = [Q(-h'(\xi))]' - [\dot{x}_\mathrm{f}(t) + Q(-h'(\xi))]h'(\xi)\sqrt{t}, \tag{2.32}$$

where $\dot{x}_\mathrm{f}(t) := \mathrm{d}x_\mathrm{f}(t)/\mathrm{d}t$ is the shock speed.

Since we are interested in the behaviour of the solution in the neighbourhood of the point $\xi = 0$, the last term on the right-hand side of (2.32) can be neglected. Indeed, using the Rankine–Hugoniot condition for the shock speed, we obtain by the analogy with (2.20), that

$$\dot{x}_{\rm f}(t) = \frac{-u(x_{\rm f}-0,t)Q(u_x(x_{\rm f}-0,t)/u(x_{\rm f}-0,t))+0}{u(x_{\rm f}-0,t)-\varepsilon} = -Q\left(\frac{u_x}{u}\right)\Big|_{x=x_{\rm f}-0} + \mathrm{O}(\varepsilon)$$
$$= -Q(-h'(0)) + \mathrm{O}(\varepsilon). \tag{2.33}$$

On the other hand, the Taylor expansion of the function $Q(-h(\xi))$ about $\xi = 0$ yields

$$Q(-h'(\xi)) = Q(-h'(0)) - \xi Q'(-h'(0))h''(0) + \mathrm{O}(\xi^2). \tag{2.34}$$

Substituting (2.33) and (2.34) into (2.32), we obtain

$$\tfrac{1}{2}(h'(\xi)\xi - h(\xi)) = [Q(-h'(\xi))]' + \xi Q'(-h'(0))h''(0)h'(\xi)\sqrt{t} + \mathrm{O}(\varepsilon+\xi^2). \tag{2.35}$$

We will seek solutions of (2.27) and (2.29) that have an infinite derivative at $x = x_{\rm f}(t)$, i.e. $\lim_{x\to x_{\rm f}-0} u_x(x,t) = \infty$. This implies that $\lim_{\xi\to 0-0} h(\xi) = \infty$, and therefore, since Q is an increasing bounded function, $Q'(-h'(0)) = 0$. Taking this into account and discarding the $\mathrm{O}(\varepsilon+\xi^2)$ terms on the right-hand side of (2.35), we arrive at the following ODE:

$$h(\xi) - h'(\xi)\xi = 2[Q(h'(\xi))]'. \tag{2.36}$$

This equation was previously considered in [26, 27]. It was shown there that one can obtain a solution of (2.36) in the form

$$h(\xi) = h(0) + A\xi^{\alpha} + \mathrm{O}(\xi^{\alpha}) \tag{2.37}$$

with $\alpha = (\beta-2)(\beta-1)$. It is easy to see that $0 < \alpha < 1$, and the discontinuity is preserved for awhile. More precisely, the discontinuity will disappear only after

$$t^* = \left[\frac{\ln(U_0/\varepsilon)}{h(0)}\right]^2.$$

Now, if $\varepsilon \to 0$ then $t^* \to \infty$, and we obtain a discontinuous solution of the IVP (2.27) and (2.28), which is of the form

$$u(x,t) = \begin{cases} U_0\,\mathrm{e}^{-\sqrt{t}h(\xi)}, & \text{if } x < x_{\rm f}(t), \\ 0, & \text{if } x > x_{\rm f}(t) \end{cases}$$

in a small vicinity of the shock front[4].

Remark. The phenomenon of delayed resolution of discontinuities is not unlike the one observed for equation (1.5) in [26, 12], with the main difference being that here the discontinuity persists indefinitely while the initial discontinuity in the IVP (1.5) and (2.28) disappears within a finite time.

3. Concluding comments

Two main issues were left for future studies.

(1) *Higher dimensions*. Though the details of propagation must change with dimension the main effect of formation of discontinuities is expected to prevail. An interesting interplay between the different dimensions is possible if one takes, say

$$u(t=0,x,y) = \cos x \cos^4 y.$$

The delay mechanism in the x and y directions differs significantly from each other and initially the motion of the front will be anisotropic.

[4] Local self-similar regimes that do not occur uniformly in the whole region of motion but only close to the front $x_{\rm f}(t)$, were considered earlier for a different class of problems in [9, 11].

(2) *The convective effects*. We have seen in previous studies [20, 17] that convection in saturating diffusion adds an important element to the dynamics. It may induce a persisting pattern (as opposed to decaying ones in the saturated diffusive processes) like travelling waves embedded with subshocks.

Acknowledgments

The problems studied in this paper were first initiated over ten years ago by P Rosenau and R W Cox. The third author is grateful to R W Cox for helping him to realize the richness of the structures resulting from the saturation of fluxes. The research of AC was supported in part by the Office of Science, Office of Advanced Scientific Computing Research, Mathematical, Information, and Computational Sciences Division, Applied Mathematical Sciences Subprogram, of the US Department of Energy, under Contract # DE-AC03-76SF00098 and by the NSF grant # DMS-9732710. The research of AK was supported in part by the NSF Group Infrastructure Grant and by the NSF Grant # DMS-0196439. The research of PR is supported in part by the Israel Science foundation Contract # 558/99-2.

Appendix A

A derivation of the saturated diffusion used in this paper was given in [23]. Here we provide an alternative derivation. The idea is as follows: any flux driving diffusion has an upper bound. Particles cannot travel faster then in a free flight. Thus given a classical, gradient driven flux $\boldsymbol{q} = -D_0(u)\boldsymbol{\nabla u}$, where $\boldsymbol{u}$ is, say, particle density, the upper limit for transfer is given via $\boldsymbol{q}_* = C\boldsymbol{u}$ where C is the free streaming speed and may itself depend on concentration. To construct a flux function that interpolates between the low gradient and the upper limit, we remember that the effective flux magnitude cannot depend on the direction. To this end, we define the effective flux function $\boldsymbol{q}_{\text{eff}}$ via second order harmonic average

$$\frac{1}{q_{\text{eff}}^2} = \frac{1}{q^2} + \frac{1}{q_*^2}.$$

Thus,

$$u_t + \operatorname{div}(\boldsymbol{q}_{\text{eff}}) = 0,$$

where

$$\boldsymbol{q}_{\text{eff}} = \frac{-D_0(u)\boldsymbol{\nabla u}}{\sqrt{1 + (D_0\nabla u)^2/(Cu)^2}}.$$

This coincides with our earlier result in [23]. To bring it to the form used in this paper, we define

$$g(u) = \int \frac{D(u)}{uC(u)}\mathrm{d}u, \qquad \boldsymbol{S} = g'(u)\boldsymbol{\nabla u}, \qquad \boldsymbol{Q}(\boldsymbol{S}) = \frac{\boldsymbol{S}}{\sqrt{1+S^2}},$$

then

$$u_t = \operatorname{div}[uC(u)\boldsymbol{Q}(\boldsymbol{S})].$$

In particular, consider diffusion of thermal pulse in gas where θ is the temperature then, assuming that $D_0(\theta) \cong \theta^m$, $C^2 \sim \theta$ we obtain $\boldsymbol{S} \sim \theta^{m-3/2}\nabla\theta$. Thus, in the normalized units

$$\theta_t = \operatorname{div}[\theta^{3/2}\boldsymbol{Q}(\boldsymbol{S})].$$

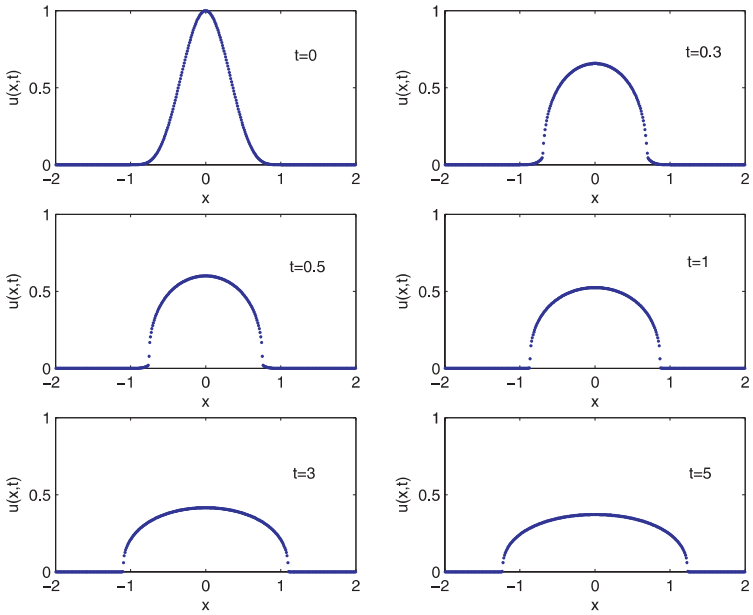

Figure A1. The solution of (A.1) and (2.4).

Two values of m are notable: neutral gas wherein $m = \frac{1}{2}$, and $\frac{5}{2}$ for a fully ionized plasma. It can be easily seen that for any $m > 0$ the saturating mechanism is active on the front. Indeed, assume to the contrary that it is not and let ζ measure the local coordinate on the front, then in its vicinity $\theta \sim \zeta^{1/m}$ and $|\boldsymbol{S}| \sim \zeta^{-1/m} \to \infty$ as ζ vanishes. Hence, the radical diverges which contradicts the assumption.

Let us mention the particulars of two cases:

(1) A neutral gas wherein $S = \theta_x/\theta$ (this case is discussed in section 2.4).
(2) The case of a fully ionized plasma wherein $S = \theta\theta_x$, the effect of classical waiting time will be even more enhanced than case $\mathcal{B}$ (section 2.2.2). Indeed, consider again initial conditions (2.4), then figure A1 describes its evolution via

$$u_t = \left[\frac{u^{5/2}u_x}{\sqrt{1+(uu_x)^2}}\right]_x. \tag{A.1}$$

Appendix B

As has been demonstrated in the numerical examples, presented in sections 2.2–2.4, the discontinuities, developed in the studied models, propagate and their amplitudes typically decrease in time. This makes it sometimes difficult (see, e.g. figures 17 and 18) to numerically capture solutions of equation (1.1).

In this paper, we have used a simple second-order central-difference semi-discrete scheme, which, for example, for equation (2.1), takes the form:

$$\frac{\mathrm{d}}{\mathrm{d}t}u_j(t) = \frac{1}{\Delta x}\left[\left(\frac{u_{j+1}(t)+u_j(t)}{2}\right)^n Q\left(\frac{u_{j+1}(t)-u_j(t)}{\Delta x}\right) - \left(\frac{u_j(t)+u_{j-1}(t)}{2}\right)^n Q\left(\frac{u_j(t)-u_{j-1}(t)}{\Delta x}\right)\right]. \tag{B.1}$$

Here, $x_j = j\Delta x$ is a spatial grid, and $u_j(t) \approx u(x_j, t)$. In a general case, a modification of the scheme is straightforward, though it will depend on a specific form of $g(u)$.

Thanks to the parabolicity of equation (2.1), it is easy to prove that this scheme, supplemented with a stable ODE solver, say the second-order modified Euler method, is stable under an appropriate CFL condition. To obtain an efficient fully discrete method, we have used the explicit large stability domain Runge–Kutta ODE solvers, recently proposed in [22, 3, 1, 2].

However, an (excessive) numerical dissipation present at the scheme (B.1) may not allow to achieve a satisfactory resolution of the discontinuities, especially at large times. This can be clearly seen in the numerical examples, presented in figures 17 and 18, where the discontinuities are smeared, and it is impossible to conclude whether the computed solution is discontinuous or not.

One may wish to use a high-resolution finite-volume scheme to improve the quality of the computed solutions. Unfortunately, the existing 'machinery' is developed for capturing shocks, that are formed due to the presence of nonlinear convection terms, as in the case of hyperbolic conservation laws. But the nature and the evolution of the front discontinuities in the studied models is different, and thus another type of method should be developed for such strongly degenerate parabolic equations as (1.1).

We are currently working on the development of a highly accurate generalization of the diffusion-velocity particle method [16, 21] for degenerate parabolic equations [14].

References

[1] Abdulle A 2002 Fourth order Chebyshev methods with recurrence relation *SIAM J. Sci. Comput.* **23** 2041–54

[2] Abdulle A ROCK4 code, htpp://www.unige.ch/math/folks/hairer/software.html

[3] Abdulle A and Medovikov A 2001 Second order Chebyshev methods based on orthogonal polynomials *Numer. Math.* **90** 1–18

[4] Aronson D G 1970 Regularity properties of flows through porous media: the interface *Arch. Rat. Mech. Anal.* **37** 1–10

[5] Aronson D G 1970 Regularity properties of flows through porous media: the counterexample *SIAM J. Appl. Math.* **19** 300–7

[6] Aronson D G, Caffarelli L A and Kamin S 1983 How an initially stationary interface begins to move in porous medium flow *SIAM J. Math. Anal.* **14** 639–58

[7] Aronson D G, Caffarelli L A and Vazquez J L 1985 Interfaces with a corner point in 1-D porous medium flow *Commun. Pure Appl. Math.* **38** 375–404

[8] Aronson D G and Serrin J 1967 Local behavior of solutions of quasilinear parabolic equations *Arch. Rat. Mech. Anal.* **25** 81–122

[9] Barenblatt G I 1996 *Scaling, Self-similarity, and Intermediate Asymptotics* (Cambridge: Cambridge University Press)

[10] Barenblatt G I 1952 On some unsteady motions of a liquid or a gas in a porous medium *Prikl. Mat. Mech.* **16** 67–78

[11] Barenblatt G I, Entov V M and Ryzhik V M 1990 *Theory of Fluid Flows Through Natural Rocks* (Dordrecht: Kluwer)

[12] Bertsch M and Dal Passo R 1992 Hyperbolic phenomena in a strongly degenerate parabolic equation *Arch. Rat. Mech. Anal.* **117** 1–32

[13] Caffarelli L A and Friedman A 1979 Regularity of the free boundary for the one dimensional flow of gas in a porous medium *Am. J. Math.* **101** 1193–218

[14] Chertock A and Kurganov A Diffusion-velocity particle method for strongly degenerate parabolic equations, in preparation

[15] Dal Passo R 1993 Uniqueness of the entropy solution of a strongly degenerate parabolic equation *Commun. Partial Diff. Eqns* **18** 265–79

[16] Degond P and Mustieles F J 1990 A deterministic approximation of diffusion equations using particles *SIAM J. Sci. Stat. Comput.* **11** 293–310

[17] Goodman J, Kurganov A and Rosenau P 1999 Breakdown in Burgers-type equations with saturating dissipation fluxes *Nonlinearity* **12** 247–68
[18] Kalashnikov A S 1967 Formation of singularities in solutions of the equation of nonstationary filtration *Z. Vychisl. Mat. i Mat. Fiz.* **7** 440–4
[19] Knerr B F 1977 The porous medium equation in one dimension *Trans. Am. Math. Soc.* **23** 381–415
[20] Kurganov A and Rosenau P 1997 Effects of a saturating dissipation in Burgers-type equations *Commun. Pure Appl. Math.* **50** 753–71
[21] Lacombe G and Mas-Gallic S 1999 Presentation and analysis of a diffusion-velocity method *ESAIM Proc., 7, Soc. Math. Appl. Indust. (Paris)* pp 225–33
[22] Medovikov A A 1998 High order explicit methods for parabolic equations *BIT* **38** 372–90
[23] Rosenau P 1992 Tempered diffusion: a transport process with propagating fronts and inertial delay *Phys. Rev.* A **46** 7371–4 (Rapid Communication)
[24] Rosenau P Diffusion models with saturated diffusion, unpublished
[25] Rosenau P 1990 Free energy functionals at the high gradient limit *Phys. Rev.* A **41** 2227–30
[26] Rosenau P, Hagan P, Northcutt R and Cohen D 1989 Delayed diffusion due to flux limitation *Phys. Lett.* A **142** 26–30
[27] Rykov Yu G 2000 Discontinuous solutions of some strongly degenerate parabolic equations *Russ. J. Math. Phys.* **7** 341–62
[28] Zeldovich Ya B and Barenblatt G I 1958 The asymptotic properties of self-modeling solutions of the nonstationary gas filtration equation *Sov. Phys.—Dokl.* **3** 44–7